The Recurrence of Atmospheric Blocking

Ka Ying Ho , Lei Wang *

Purdue University, Department of Earth, Atmospheric, and Planetary Sciences, West Lafayette, IN, United States

Edwin P. Gerber

Courant Institute of Mathematical Sciences, New York University, New York, NY, United States

Yi Ming

Schiller Institute for Integrated Science and Society and Department of Earth and Environmental Sciences, Boston College, Chestnut Hill, MA, United States

Corresponding author: Lei Wang, leiwang@purdue.edu

ABSTRACT

Blocking is a persistent, large-scale circulation pattern in the mid-latitude atmosphere associated with extreme weather at the surface. Identifying and understanding the temporal evolution of blocks is not only important for enhancing our capability to predict them, but also for shedding light on whether atmospheric blocking is a distinct meteorological phenomenon. This study examines the recurrence, or return period distribution of blocking in the Northern Pacific, Northern Atlantic, and Southern Pacific regions for both warm and cold seasons. Using ERA5 reanalysis data and Community Earth System Model Large Ensemble (CESM LENS) outputs, this study finds that blocking events are typically seperated from each other on a timescale of 8-12 days, which is robust across regions and seasons. The recurrence distributions are interpreted with a hierarchy of one and two dimensional stochastic models. The idealized models indicate that the variation in blocking recurrence depends on the climatological onset frequency of blocking events and the characteristic temporal correlation of Rossby waves. The return period distributions in reanalysis and CESM are consistent with an AR(1) autoregressive process of order 1 model, suggesting that the temporal structure of blocks can be interpreted as red noise associated with synoptic variability. Using the CESM LENS outputs, the authors find that the decline in blocking frequency in a warmer climate leads to a broader spread of the return-period distribution, increasing variance in the recurrence of blocks.

Significance statement. Atmospheric blocking is a large-scale weather pattern in the midlatitudes associated with various types of extreme events, such as heat waves, droughts, and cold spells. Understanding its regularity in time can help us better predict its onset and understand the forecast limit of blocking. Using a hierarchy of simple red-noise models, we identify the key parameters that contribute to the recurrence pattern of blocking, specifically, the climatological onset frequency and the temporal correlation of Rossby waves, which shape the return period distribution and timescale. These insights also help interpret changes in the pattern of recurrence and forecast challenges in a warmer climate from the CESM1 simulations, where a decrease in blocking events increases the uncertainty of their recurrence.

1. Introduction

Atmospheric blocking is an important phenomenon characterized by the stagnation of propagating weather systems and often leads to surface extremes (Kautz et al. 2022) such as heat waves (Brunner et al. 2018; Neal et al. 2022; Pfahl and Wernli 2012), cold spells (Brunner et al. 2018; Demirtaş 2017), and extreme precipitation. As blocks occur on a timescale longer than the typical synoptic weather, but shorter than seasonal variations, understanding their temporal evolution can help bridge the gap between weather and climate extremes and mend the weather-climate schism (Randall and Emanuel 2024). Current short- or medium-range forecasts do not adequately predict blocks, making extremes more dangerous, especially in a changing climate (Intergovernmental Panel On Climate Change 2023).

The spatial distribution of blocks is well-understood: in the Northern hemisphere, blocks are found more frequently over the Northern Pacific, Northern Atlantic, and Greenland (Dole and Gordon 1983; Tyrlis and Hoskins 2008; Woollings et al. 2018). In the Southern Hemisphere, blocks are primarily observed over the South Pacific (Liu and Wang 2024). However, less is known

about the temporal features of blocks. As a recent Perspective (Wang et al. 2026) pointed out, among blocking detection algorithms, nearly all identify blocks when the usual westerly flow is blocked in a region for five days or more. Beyond the 5-day temporal threshold for blocks, however, we do not have much understanding of the temporal features of blocks. This study aims to provide more insight of blocking events by exploring the regularity in its occurrence. We ask how blocking events are interspersed in time, whether there is more regularity than weather noise, and how this variability differs among regions, and between observations and models.

The presence of any regularity in blocking occurrence would help us to understand the fundamental processes behind the phenomenon. For example, if blocks are driven primarily by feedback processes from random synoptic eddies' (Shutts 1983), then a null-hypothesis is that their temporal structure is largely random, their onset following the distribution of synoptic eddies, but with events exhibitng extended persistence due to the self-sustaining nature of the blocks. This begs the question, how do blocks differ from random noise? By definition, blocks are larger in size and longer lasting than random eddies, as well documented in classic diagnostic works, e.g. Dole and Gordon (1983). But if the main distinctions between blocks and individual weather systems are just size and duration, the distinction would be purely semantic rather than fundamental. Masato et al. (2009) demonstrated that a simple first-order Markov model, with observed coherence included in its formulation, can reproduce the main features of blocking frequencies. The only exception is that observed blocks appear to be more persistent than predicted by the first-order Markov model. Recent studies have shown the importance of diabatic heating (Pfahl et al. 2015; Liu and Wang 2025) and baroclinic energy exchange from synoptic systems (Martineau et al. 2022) in the maintenance of block.

In exploring the temporal patterns of atmospheric blocking, earlier studies have linked blocking with various internal modes of variability, which include the zonal wind cycle (Namias 1950;

Rossby 1939), Northern Annular Mode (Tachibana et al. 2010; Thompson and Wallace 2000) and North Atlantic Oscillation (Scherrer et al. 2006). Liu and Wang found that the Baroclinic Annular Mode (BAM), a leading mode of storm activity with a periodicity of 20-30 days, modulates the frequency of atmospheric blocking (Liu and Wang 2023; Liu 2023). The alignment of blocking with a periodic annular mode implies that blocking occurrence may exhibit more regularity than red noise. Indeed, blocks and associated extremes are associated with slowly propagating Rossby wave packets with an intrinsic timescale of 10 days (Castañeda and Wang 2024; Röthlisberger and Martius 2019; Teng et al. 2013; Wirth et al. 2018). Despite evidence suggesting potential regularity in blocking occurrence, the temporal variability and recurrence of blocks have not yet been systematically examined. It remains unclear whether blocks exhibit a characteristic return period and how this compares with that of typical synoptic eddies. Recognizing the preferred recurrence of blocks at specific timescales could potentially provide a largely underexploited intrinsic predictability of blocks and improve medium-range weather forecasts in current and future climates. Further, this could provide key ingredients for us to re-think the first-order dynamics of atmospheric blocking. This work investigates the recurrence of blocks based on observations and a climate model, aided by insights from simple red noise models.

We evaluate to what extent blocking exhibits a regular recurrence pattern in several key regions of blocks, including the Northern Pacific, Northern Atlantic, and Southern Pacific regions, in both warm and cold seasons, and we compare the statistics to those in two simple red noise models: the 2-D model of Masato et al. (2009) and an even simpler 1-D model. The methodology, including blocking detection, corresponding return period calculation, and red noise model construction, are elaborated in Section 2, followed by a discussion of the results from observation, climate model, and red noise models in Section 3. Our conclusions are in Section 4.

2. Data and Methods

a. Reanalysis and Climate Model Outputs

The blocking analysis performed in this study uses the ERA5 reanalysis dataset from the European Centre for Medium-Range Weather Forecasts (ECMWF, Hersbach et al. 2020). We use the daily mean geopotential height field at 500 hPa (Z500) from 1 January 1940 to 31 December 2022 with $1^\circ \times 1^\circ$ horizontal resolution to diagnose blocking events. We also evaluate historical and potential future changes in blocking recurrence using daily model outputs from the Community Earth System Model version 1 (CESM1). We analyze blocks from the LENS integrations of the fully-coupled CESM1 under preindustrial radiative forcing, as well as future climate scenarios (RCP 8.5), with 30 ensemble members each (Deser et al. 2020).

b. Blocking Detection and Return Period Calculation

To analyze blocking events, we calculate the Local Wave Activity (LWA) by integrating the meridional displacement of the Z500 contour (Chen et al. 2015; Huang and Nakamura 2016),

$$LWA_{Z500}(t,\phi,\lambda) = \frac{a}{\cos\phi_{eq}}\left(\int_{\phi\le\phi_{eq}} z'\cos\phi d\phi - \int_{\phi\ge\phi_{eq}} z'\cos\phi d\phi\right) \quad (1)$$

where a is the radius of the earth, ϕ_{eq} is the equivalent latitude. The equivalent latitude encloses the same area for a given Z500 contour. z' denotes the deviation of Z500 from its value at ϕ_{eq}.

LWA attains a large value whenever the deformation of Rossby wave is significant, thus blocking events can be identified by the detection algorithm similar to that in Liu and Wang (2024). In particular, when the LWA at a location exceeds a threshold relative to its climatology, a wave event can be identified and tracked by the longitude of peak LWA. We define the LWA threshold by first identifying the maximum observed value at each longitude, and then taking the

median of them. A blocking event is then defined when a wave event remain quasi-stationary (propagates less than of 13.5^0 in latitude and 18^0 in longitude per day), and persists for at least 5 days.

The return period is defined as the time difference between the onsets of consecutive blocking events within a given region. Figure 1 provides an example of the evolution of Z500 and LWA during two successive blocking events over the North Atlantic. The events are identified by the locations of maximum LWA, indicated by yellow crosses. The first event began on 29 June 1985 (marked by the blue box) and persisted for 6 days. Twelve days after its onset, a second blocking event occurred in the same region on 11 July 1985. The distribution of such recurrence in blocking events thus characterizes the timescale over which the atmosphere returns to a blocked state in a given region. A strongly peaked recurrence distribution indicates that blocking events return with high regularity.

The LWA-based blocking climatology for summer (JJA) and winter (DJF) is shown in Figure 2. The main blocking regions over the Northern Pacific, Northern Atlantic, Greenland and Southern Pacific are clearly identified, consistent with patterns and frequency obtained using different blocking metrics (see a review from Woollings et al. (2018), Masato et al. (2013)). The latitudinal and longitudinal extent of the regions of focus in this study are listed in Table 1. We do not consider blocks over Greenland, as our red noise model is not well suited to capture the influence of topography on these blocks.

c. Red Noise Models

1) An ERA5-constrained 2D model

Inspired by the red noise model developed by Masato et al. (2009), we construct a similar two-dimensional (2D), i.e., longitude and time, red noise model, modified slightly to better fit the LWA

data. To be consistent with observed temporal and spatial coherence, the model is calibrated from the daily LWA data at 50° N/S at 5° spatial resolution in longitude. The goal is to simulate the anomalous LWA, ΔW, as a function of longitude and time. It is built on the equations,

$$\begin{aligned} \Delta W_n^* &= \phi \cdot \Delta W_{n-1} + \epsilon_n \\ \Delta W_n &= \mathbf{A} \Delta W_n^* \end{aligned} \tag{2}$$

where the vector ΔW_n is the deviation of LWA from its climatological mean at each longitude at a given time step n, ϕ is a longitude-dependent vector, the lag-1 temporal autocorrelation of each longitude computed from the data, and ϵ_n is a vector of white noise. The matrix A is empirically derived to capture the observed spatial correlation pattern across longitudes, based on how each point (5° of longitude) is correlated to its three neighboring points. It is therefore mostly zero except for the 7 principal diagonals.

The details of model construction, as well as its temporal and spatial correlations, are provided in Appendix A. Its statistics is a well match of the correlation patterns observed in ERA5.

Figure 3(a) shows the Hovmöller diagram of LWA in ERA5 data during 1985 JJA, the period of Northern Atlantic blocking episodes shown in Figure 1. The onset of blocking events are marked with crosses, and are also represented as a 1D time series to highlight their temporal distribution. The same analysis from the ERA5-constrained 2D red noise model is presented in Figure 3(b), where the LWA threshold for blocking has been adjusted to ensure the red noise model has the same climatological frequency of events as observed. The red noise model accurately captures the temporal and spatial coherence of the observation, particularly in terms of the duration and size of wave events. With the absence of jet stream and Rossby wave dynamics in the red noise model, however, “wave events” propagate both eastward and westward in a random fashion.

2) 1D and 2D conceptual models

To investigate the roles of temporal and spatial parameters in shaping blocking recurrence patterns, a set of simplified red noise models are constructed. First, we consider a very simple, first auto-regressive (AR-1) model to describe the evolution of LWA in time only, governed by

$$\Delta W_n = \phi \cdot \Delta W_{n-1} + \epsilon_n \tag{3}$$

where ΔW_n represents the deviation of LWA from its climatological mean at a single grid point and time step n, ϕ is the lag-1 temporal autocorrelation coefficient, and ϵ_n is a white noise time series. The 1D model represents the simplest framework for describing the temporal pattern of blocking events. In this formulation, only the temporal correlation ϕ and the total number of events, or onset frequency (set by the blocking threshold, or equivalently, amplitude of the noise), influence the distribution of blocks.

A second 2D conceptual model shares the same equation 2 as the ERA5-constrained models, but with a simplified spatial correlation matrix A. The diagonals of matrix A are uniform across longitudes. This makes the variability statistically uniform in longitude, allowing us to explore the effect of domain size on the recurrence distribution.

3. Results

a. Blocking recurrence statistics in reanalysis

To investigate the structure of blocking recurrence, we analyze the LWA during blocking events and the probability distribution of the blocks preceding and proceding a given event. The composites of LWA for all blocking events in JJA and DJF (with onset within the respective

season) are shown as red shading in the Hovmöller diagrams in Figure 4. The Hovmöller diagram is centered on the tracking longitude at onset (i.e., maximum point of LWA), and LWA is averaged over ±5° in latitude relative to it. The resulting composites highlight the temporal and spatial characteristics of LWA during blocking events, exhibiting a pronounced peak at day 0, reflecting the stationarity and persistence of blocking.

To quantify where and when the preceding and proceeding blocking events occur, we composite the binary LWA masks of blocks occurring before and after each event, shown as purple shading. The fraction of times where the flow was previously/next blocked exhibits local maxima approximately 5–15 days before and after the reference event across all regions and in both seasons.

During boreal summer, pre- and proceeding blocks are more likely for Northern and Southern Pacific blocks compared to the Northern Atlantic blocks, reflecting the higher overall blocking frequency. Northern Pacific blocks have a more intense recurrence peaking at around 8-10 days, whereas the Southern Pacific blocks exhibit recurrence across a broader timescale, ranging from 5-15 days. The recurrence signal is weaker in the Northern Atlantic over the range of 8-15 days, where synoptic variability dominates the high-latitudes. In contrast, the recurrence during winter for the Northern Pacific and Southern Pacific blocks is weaker and more dispersed compared to that in summer. Recurrence across longer timescale are observed, which break into several sub-peaks ranging from 5 to 17 days. This is consistent with the strong winter jet that advects wave activity eastward during winter. However, the recurrence for Northern Atlantic blocks becomes stronger during winter, peaking at a shorter timescale of 5-10 days, that is a defluent region where advection does not dominate.

Figures 5 and 6 show the return period distribution of blocks for ERA5 and the 2D red noise model in the Northern Pacific, Northern Atlantic, and Southern Pacific during boreal/austral summer and

winter. Return period is defined as number of days between the onsets of consecutive blocking events within the region. The corresponding Kernel density estimations (KDE) are plotted in the right panels (b), which attempt to reduce the sampling uncertainty. In the Northern Hemisphere, blocking events are more active in the Northern Pacific, where they persist longer and recur more frequently (see details of blocking durations and recurrence in Table 3). The peak of recurrence for the Northern Pacific blocks is more pronounced at 8.4 days. The Atlantic blocks return with a wider range with a peak at 11.4 days, while the Southern Pacific blocks exhibit a distinct peak of recurrence at 9.9 days. The enhanced recurrence peak in the Southern Pacific within sub-seasonal-to-seasonal frequency range may reflects the influence of the quasi-periodic annular mode (Liu and Wang 2023). The winter return period of blocks in the South Pacific shows a larger spread with a less distinct peak, consistent with the Hovmöller composite diagram in Figure 2. Both Northern Pacific and Northern Atlantic blocks have a shorter recurrence at 8.1 and 8.9 days, respectively. Recurrence at 11.9 days in the Southern Pacific appears weaker and more prolonged during winter.

The recurrence signal remains strong when using 4-day and 6-day blocking thresholds (results not shown), with the peak slightly shifting to 7–10 days and 10–18 days, respectively, due to changes in the total number of detected events. The dependence of the recurrence pattern on onset frequency and temporal correlation will be established in Session 3c. The choice of the 5-day threshold is consistent with the convention in the community, but modifying it does not change the physical insights of our results appreciably - affecting the return period distribution must exclusively by influencing the blocking rate.

b. The blocking recurrence response to climate change

Using the CESM1 model, we extend our blocking analysis to 1,799 years of data from the preindustrial control simulation and evaluate the blocking response to a warmer climate using 600

years of data from the RCP8.5 simulation. The spatial patterns of the observed blocking regions are well captured by this climate model.

Figure 7 shows the model bias from CESM1 preindustral run simulation from (a) JJA and (b) DJF. Compared to ERA5, the rate of which the flow is blocked in CESM1 is higher in the Northern Pacific in both JJA and DJF, as well as in the Southern Pacific in JJA. Despite exihibiting an overall higher frequency of blocked states, CESM1 exihibits fewer blocking events because its events persist longer, see Table 3.

Figure 8 shows the response of the CESM1 block frequency in a warmer climate. The model projects a decrease in most blocking regions, with the exception of Greenland summer blocks and Pacific winter blocks over the Gulf of Alaska. In a warmer climate, the challenge posed by blocking-associated surface extremes lies less in changes in event frequency and more in the increased unpredictability of rare events. The implications of changes in blocking frequency for recurrence patterns are discussed further in a later section with insights drawn from the red noise model.

Figure 9 shows the return periods of blocking events from the CESM1 model, where the green and orange histograms represent results from the preindustrial control run and the RCP 8.5 run, respectively. To account for differences in sample size, the preindustrial simulation is subsampled into 600-year segments 100 times, and the results remain consistent and robust. The 8-12 day peak of recurrence can be observed among blocking events of CESM1.

To quantify differences in return-period distributions between the preindustrial and future climates, we applied the Kolmogorov–Smirnov (KS) and Kullback-Leibler divergence test (KL div). The KS p-values are computed as the mean over 10,000 tests based on different subsamples of the data. As shown in Table 5, with the exception of Northern Pacific JJA blocks, the p-values exceed 0.05 in all regions and seasons, indicating that there are no statistically significant differences in

the return-period distributions in a warmer climate. The frequency of onset in the Northern Pacific during JJA shows the largest decline, such that the null hypothesis of no change can be rejected.

c. Conceptual understanding of blocking recurrence from red noise models

1) Recurrence in red noise models

Despite the mechanistic differences between observed blocking events and those generated by red noise, the recurrence of blocking can largely be explained by a red noise process (AR-1). Unlike Masato et al. (2009), who identified a distinct distribution pattern for the durations of blocks, we find that the return distribution of blocking is indistinguishable from an AR-1 process.

Table 4 lists the results of the statistical tests for the distributions of the return period in ERA5 and the red noise model. As the sample sizes of ERA5 and the model are vastly different (82 vs 20,000 years), the KS test has been repeated 10,000 times on sub-samples from the model. The p-values obtained are the mean across all tests. In addition, KL-div test has been carried out to quantify the differences between the KDEs from ERA5 and the model.

The return period distributions from ERA5 and the red noise model are statistically indistinguishable for the Northern Pacific and Atlantic blocks from both seasons. The p-values are above the typical significance threshold, 0.05, indicating that the observations and the models likely come from the same distribution. In contrast, we can reject the null hypothesis that blocking recurrence in Southern Pacific in both seasons comes from the same distribution as the red noise model, with p-values lower than 0.05. With less zonal asymmetry in the Southern Hemisphere, blocking events in the Southern Pacific exhibit more temporal regularity, consistent with findings in Liu and Wang (2024) that blocking events in the region are enhanced by the quasi-periodic baroclinic annular mode. By and large, however, the red noise model captures the observed recurrence timescale and

overall distribution, offering conceptual insight into the processes that shape the temporal structure of blocking occurrence.

2) Temporal factors from 1D model

In a 1D model where LWA evolves in time at a single grid point, the blocking return periods are determined by the model's temporal correlation and the onset frequency, defined by the total number of onsets over the number of days. Onset frequency is a convenient metric that can be measurable from observational data and is applicable to any blocking algorithm. The return period quantifies the temporal distribution of events, and the total number of onsets determines the mean spacing between successive events. To demonstrate the role of temporal parameters in blocking recurrence, we generate 200,000 years of data using 1D red noise models, with onset frequency, α = Total number of onsets/Total number of days, ranging from 1 to 9%, and temporal correlation coefficient from 0.1 to 0.8. Figure 10(a) shows the recurrence (i.e., the KDE peak of the return period distributions) across different onset frequencies, and the temporal correlation coefficients of 1D model runs. For an onset frequency below 2%, the peak of recurrence remains around 16 to 18 days and varies little with temporal correlation. When probability of blocking is low, the return period distributions flatten (not shown) and skew towards the mean return period. Within the observed onset frequency range of 3-6%, the recurrence peaks show a stronger dependence on the temporal correlation, shifting toward a longer timescale as the temporal correlation increases. A stronger temporal correlation leads the model to persist in a given state for longer periods, thereby increasing the longevity of blocks and the time interval between blocking events. In particular, despite the simplicity of the 1D model, the observed 8–12-day recurrence time scale falls broadly within this onset-frequency regime.

Figure 10 also shows the return period distributions for (b) varying onset frequency with fixed temporal correlation of 0.7, and (c) varying temporal correlation with fixed onset frequency of 5%. The values $\phi = 0.7$ and $\alpha = 5\%$ fall within the observed range from ERA5 (see details of observed ϕ and α in Table 4). Though the recurrence peaks remain largely within the 8-12 time window, the spreads and tails of the distributions vary substantially and are particularly sensitive to changes in onset frequency, where lower onset frequencies correspond to wider distributions. The dependence of distribution spread on onset frequency is also evident in the distribution of blocks in ERA5, as shown in Figures 5 and 6. Temporal correlation contributes to the spread and skewness of the distribution, with stronger temporal correlation corresponding to a wider and more centrally peaked distribution.

In the CESM1 simulations, the flattening of the return-period distribution for Northern Pacific JJA blocking in a warmer climate is associated with a nearly 1% reduction in onset frequency. Changes in temporal correlation or onset frequency smaller than 1% do not appear to produce statistically significant changes in the distribution.

3) The impact of domain size on recurrence

Using the zonally uniform 2D red noise models with varying domain sizes, we investigate the spatial factors that affect the return period distribution of blocking. Similar to the 2D model constructed for ERA5, ΔW anomalies are spatially correlated to the neighboring three points (i.e., 15º), but with uniform spatial correlation coefficient across longitudes (matrix A in Eq. 2 is uniform across longitudes). This modification is introduced for the convenience of varying the domain size. Note that our blocking detection algorithm does not impose any threshold on blocking size. Therefore, by varying the domain size in the model, we can examine both how recurrence changes with the size of blocking regions and how it depends on spatial coherence.

Results obtained from larger domain sizes can also be interpreted as representing domains with weaker spatial coherence and smaller blocking structures. The 2D models have been run for 20,000 years, with domain sizes ranging from 40° to 540° in longitude. Values exceeding 360° should be interpreted as an increasing the planetary radius which fixing the deformation radius (see domain size details in the legend of Figure 12).

Figures 11 (a) and (b) show the recurrence peak and onset frequency of the 2D models in varying domain sizes and temporal correlations. Recall from Figure 10 that the recurrence peak is inversely related to the onset frequency of the domain. Although the spatial distribution of blocks varies with domain sizes, the return period depends only on the temporal spacing between blocks, and is therefore largely controlled by the number of onsets within the domain. In other words, the general behavior of recurrence can be inferred from the climatological blocking frequency of a given domain, regardless of its spatial coherence or size.

The observed blocking basins in ERA5 correspond to a domain size of 60° longitude and temporal correlations in the range of $\phi = 0.5 - 0.7$, yielding recurrence peaks of approximately 5 to 10 days. This is close to the observed 8-12-day window, despite the simplified spatial coherence structure in the models. The upper right part of Figure 11(a) exhibits recurrence peaks of 1 day, indicative of an exponential-like distribution. Larger domain sizes favor such a distribution, such that for domain exceeding 180º (not shown), the distribution becomes exponential-like, peaking at 1 day regardless of temporal correlation. This reflects the increased blocking frequency in the lesser domain.

Figure 12 shows the onset frequency per degree of longitude for domain sizes ranging from 40° to 540°. The onset frequency increases proportionally with domain size when the domain expands from 40º to 80º, as shown by the nearly constant values in the plot. A rapid increase in onset frequency appears between 80º and 100º. This increase in blocking probability arises when the

domain becomes large enough to allow an additional blocking episode to occur simultaneously. Such transition also occurs between 36 and 48 grid points, and again between 360º and 420º.

The transition effect of the domain size is also evident in the return-period distributions (at $\phi = 0.7$) shown in Figure 13(a). At domain sizes of 40º to 80º, the distributions vary little and remain similar to AR-1 like distributions. As the domain size increases, the distribution changes drastically from 100º onward, becoming a rapidly decaying function with a peak at 1 day. This distribution resembles that of a 2D white noise model, as shown in Figure 13(b). Although the red noise model prescribes spatial correlation among neighboring points, each subsection of the domain remains spatially coherent internally, but is not effectively correlated with other subsections. With increasing domain size, the temporal pattern of blocking onsets is no longer dominated by the red-noise-like behavior of individual subsections, but instead by the collective pattern arising from all subsections, which operate independently.

4. Conclusions

Understanding the regularity of the temporal features of the blocks can help us to better predict the blocks. Using ERA5 reanalysis data and a climate model output, we find a preferential recurrence of blocks on the timescale of 8-12 days robustly across regions and seasons. We find, however, that the recurrence, or return period distribution, can be qualitatively reproduced by a simple AR(1) red-noise model. The AR(1) model shows how the recurrence distribution depends critically on the temporal correlation of synoptic variability and the rate of block onset.

An increase in the blocking frequency, for instance, associated with enhanced atmospheric variability over a given region or in response to a climate perturbation, decreases the peak recurrence timescale. The mean separation between blocks is inversely related to the rate. Increased persistence of the flow is associated with opposing effects: increasing the likelihood of an extended

blocking event, but also slowing the variation of the flow. On balance, increased persistence flattens the recurrence spectrum, tending to increase the peak recurrence period. This finding prompts us to re-think the dynamics of atmospheric blocking. That the recurrence distribution can be closely matched by an extremely simple AR(1) process suggests that blocking can be viewed as the tail end of the red spectrum of synoptic variability. Variations in the amplitude of synoptic variability (the local wave activity) still matter, as do their temporal decorrelation, as these factors set the overall blocking frequency. In future work, it would be interesting to investigate whether this recurrence can be better explained by the quasi-periodic behavior inherent in an AR(2) process – implying the importance of memory blocking dynamics — but it would likely require a very long climate integration to definitively rule out a simple red noise null hypothesis.

These findings enable us to interpret the recurrence in climate models integrations of past and future climates. CESM1's preindustrial control and and RCP 8.5 simulations exhibit consistent recurrence period distributions, suggesting no major changes in the temporal structure of blocking in response to global warming. In a warmer climate, however, the blocking frequency generally declines, leading to a broader return period distribution. While this leads to a subtle decrease in the overall risk of weather extremes associated with blocking, the return distribution will broaden out, potentially making them more challenging to forecast.

Acknowledgments. The research is funded by the NOAA award NA24OARX431C0054-T1-01. EPG acknowledges support from the NSF award OAC-2004572.

Data availability statement. The ERA5 reanalysis is available at `https://www.ecmwf.int/en/forecasts/datasets/reanalysis-datasets/era5`. The authors acknowledge the use of outputs from the CESM large-ensemble (LENS) project.

APPENDIX A

ERA5-constrained Red Noise Model

The 2D red noise model constructed extends the framework from Masato et al. (2009) to capture the observed temporal and spatial correlation of LWA from ERA5. The model is constructed at daily resolution with 5º longitude spacing. Following Equation 2, ΔW denotes the deviation of LWA from its seasonal mean, ϕ is the observed lag-1 autocorrelation, a function of longitude, and ϵ is a Gaussian white noise term, which also varies in longitude to match the observed variance.

The spatial correlation matrix A is defined and optimized in the following way: the matrix is partitioned into six longitudinal segments to represent large-scale spatial heterogeneity. The elements of A are parameterized using correlation strength, decay rate, and asymmetry. The optimal parameters are obtained by minimizing the combined error in temporal autocorrelation and zonal spatial correlation between the model and ERA5. The optimization is performed using a bounded L-BFGS-B algorithm with multiple initializations.

Figure 14 shows the temporal and spatial correlations of ERA5 (solid lines) and the ERA5-constrained 2D red noise model (dotted lines) in the Northern and Southern Hemispheres during (a–b) JJA and (c–d) DJF. Consistent with the model validation in Masato et al. (2009), the correlations produced by our red noise model qualitatively resemble those observed in ERA5.

References

Brunner, L., N. Schaller, J. Anstey, J. Sillmann, and A. K. Steiner, 2018: Dependence of Present and Future European Temperature Extremes on the Location of Atmospheric Blocking. *Geophysical Research Letters*, **45 (12)**, 6311–6320, doi:10.1029/2018GL077837, URL https://onlinelibrary.wiley.com/doi/abs/10.1029/2018GL077837, _eprint:

https://onlinelibrary.wiley.com/doi/pdf/10.1029/2018GL077837.

Castañeda, V., and L. Wang, 2024: The Role of Climatological State in Supporting US Heat Waves Through Rossby Waves Packets. *Journal of Geophysical Research: Atmospheres*, **129 (4)**, e2023JD039 212, doi:10.1029/2023JD039212, URL https://onlinelibrary.wiley.com/doi/abs/10.1029/2023JD039212, _eprint: https://onlinelibrary.wiley.com/doi/pdf/10.1029/2023JD039212.

Chen, G., J. Lu, D. A. Burrows, and L. R. Leung, 2015: Local finite-amplitude wave activity as an objective diagnostic of midlatitude extreme weather. *Geophysical Research Letters*, **42 (24)**, 10,952–10,960, doi:10.1002/2015GL066959, URL https://onlinelibrary.wiley.com/doi/abs/10.1002/2015GL066959, _eprint: https://onlinelibrary.wiley.com/doi/pdf/10.1002/2015GL066959.

Demirtaş, M., 2017: The large-scale environment of the European 2012 high-impact cold wave: prolonged upstream and downstream atmospheric blocking. *Weather*, **72 (10)**, 297–301, doi:10.1002/wea.3020, URL https://onlinelibrary.wiley.com/doi/abs/10.1002/wea.3020, _eprint: https://onlinelibrary.wiley.com/doi/pdf/10.1002/wea.3020.

Deser, C., and Coauthors, 2020: Isolating the Evolving Contributions of Anthropogenic Aerosols and Greenhouse Gases: A New CESM1 Large Ensemble Community Resource. *Journal of Climate*, **33 (18)**, 7835–7858, doi:10.1175/JCLI-D-20-0123.1, URL https://journals.ametsoc.org/view/journals/clim/33/18/jcliD200123.xml.

Dole, R. M., and N. D. Gordon, 1983: Persistent Anomalies of the Extratropical Northern Hemisphere Wintertime Circulation: Geographical Distribution and Regional Persistence Characteristics. *Monthly Weather Review*, **111 (8)**, 1567–1586, doi:10.1175/1520-0493(1983)111⟨1567:PAOTEN⟩2.0.CO;2, URL https://journals.ametsoc.org/view/journals/mwre/111/8/1520-0493_1983_111_1567_paoten_2_0_co_2.xml.

Hersbach, H., and Coauthors, 2020: The ERA5 global reanalysis. *Quarterly Journal of the Royal Meteorological Society*, **146 (730)**, 1999–2049, doi: 10.1002/qj.3803, URL https://onlinelibrary.wiley.com/doi/abs/10.1002/qj.3803, _eprint: https://onlinelibrary.wiley.com/doi/pdf/10.1002/qj.3803.

Huang, C. S. Y., and N. Nakamura, 2016: Local Finite-Amplitude Wave Activity as a Diagnostic of Anomalous Weather Events. *Journal of the Atmospheric Sciences*, **73 (1)**, 211–229, doi:10.1175/JAS-D-15-0194.1, URL https://journals.ametsoc.org/view/journals/atsc/73/1/jas-d-15-0194.1.xml.

Intergovernmental Panel On Climate Change, 2023: *Climate Change 2021 – The Physical Science Basis: Working Group I Contribution to the Sixth Assessment Report of the Intergovernmental Panel on Climate Change*. 1st ed., Cambridge University Press, doi:10.1017/9781009157896, URL https://www.cambridge.org/core/product/identifier/9781009157896/type/book.

Kautz, L.-A., O. Martius, S. Pfahl, J. G. Pinto, A. M. Ramos, P. M. Sousa, and T. Woollings, 2022: Atmospheric blocking and weather extremes over the Euro-Atlantic sector – a review. *Weather and Climate Dynamics*, **3 (1)**, 305–336, doi:10.5194/wcd-3-305-2022, URL https://wcd.copernicus.org/articles/3/305/2022/.

Liu, Z., 2023: Enhanced Occurrence of Atmospheric Blocking in the Southern Hemisphere By Baroclinic Annular Mode [Software]. Zenodo, URL https://zenodo.org/records/10140013, doi:10.5281/zenodo.10140013.

Liu, Z., and L. Wang, 2023: Regional Features of the 20–30 Day Periodic Behavior in the Southern Hemisphere Summer Circulation. *Geophysical Research Letters*, **50 (18)**, e2023GL104 256, doi:10.1029/2023GL104256, URL https://onlinelibrary.wiley.com/doi/abs/10.1029/2023GL104256, _eprint: https://onlinelibrary.wiley.com/doi/pdf/10.1029/2023GL104256.

Liu, Z., and L. Wang, 2024: Enhanced Occurrence of Atmospheric Blocking in the Southern Hemisphere by Baroclinic Annular Mode. *Geophysical Research Letters*, **51 (4)**, e2023GL107 343, doi:10.1029/2023GL107343, URL https://onlinelibrary.wiley.com/doi/abs/10.1029/2023GL107343, _eprint: https://onlinelibrary.wiley.com/doi/pdf/10.1029/2023GL107343.

Liu, Z., and L. Wang, 2025: Blocking diversity causes distinct roles of diabatic heating in the Northern Hemisphere. *Nature Communications*, **16 (1)**, 5613, doi:10.1038/s41467-025-60811-4, URL https://www.nature.com/articles/s41467-025-60811-4.

Martineau, P., H. Nakamura, A. Yamamoto, and Y. Kosaka, 2022: Baroclinic Blocking. *Geophysical Research Letters*, **49 (15)**, e2022GL097 791, doi:10.1029/2022GL097791, URL https://onlinelibrary.wiley.com/doi/abs/10.1029/2022GL097791, _eprint: https://onlinelibrary.wiley.com/doi/pdf/10.1029/2022GL097791.

Masato, G., B. J. Hoskins, and T. Woollings, 2013: Winter and Summer Northern Hemisphere Blocking in CMIP5 Models. *Journal of Climate*, **26 (18)**, 7044–7059, doi:10.1175/JCLI-D-12-00466.1, URL https://journals.ametsoc.org/view/journals/clim/26/18/jcli-d-12-00466.1.xml.

Masato, G., B. J. Hoskins, and T. J. Woollings, 2009: Can the Frequency of Blocking Be Described by a Red Noise Process? *Journal of the Atmospheric Sciences*, **66 (7)**, 2143–2149, doi:10.1175/2008JAS2907.1, URL https://journals.ametsoc.org/view/journals/atsc/66/7/2008jas2907.1.xml.

Namias, J., 1950: THE INDEX CYCLE AND ITS ROLE IN THE GENERAL CIRCULATION. *Journal of the Atmospheric Sciences*, **7 (2)**, 130–139, doi:10.1175/1520-0469(1950)007⟨0130:TICAIR⟩2.0.CO;2, URL https://journals.ametsoc.org/view/journals/atsc/7/2/1520-0469_1950_007_0130_ticair_2_0_co_2.xml.

Neal, E., C. S. Y. Huang, and N. Nakamura, 2022: The 2021 Pacific Northwest Heat Wave and Associated Blocking: Meteorology and the Role of an Upstream Cyclone as a Diabatic Source of Wave Activity. *Geophysical Research Letters*, **49 (8)**, e2021GL097 699, doi:10.1029/2021GL097699, URL https://onlinelibrary.wiley.com/doi/abs/10.1029/2021GL097699, _eprint: https://onlinelibrary.wiley.com/doi/pdf/10.1029/2021GL097699.

Pfahl, S., C. Schwierz, M. Croci-Maspoli, C. M. Grams, and H. Wernli, 2015: Importance of latent heat release in ascending air streams for atmospheric blocking. *Nature Geoscience*, **8 (8)**, 610–614, doi:10.1038/ngeo2487, URL https://www.nature.com/articles/ngeo2487, number: 8.

Pfahl, S., and H. Wernli, 2012: Quantifying the relevance of atmospheric blocking for co-located temperature extremes in the Northern Hemisphere on (sub-)daily time scales. *Geophysical Research Letters*, **39 (12)**, doi:10.1029/2012GL052261, URL https://onlinelibrary.wiley.com/doi/abs/10.1029/2012GL052261, _eprint: https://onlinelibrary.wiley.com/doi/pdf/10.1029/2012GL052261.

Randall, D. A., and K. Emanuel, 2024: The Weather–Climate Schism. *Bulletin of the American Meteorological Society*, **105 (1)**, E300–E305, doi:10.1175/BAMS-D-23-0124.1, URL https://journals.ametsoc.org/view/journals/bams/105/1/BAMS-D-23-0124.1.xml.

Rossby, R. C., 1939: Relation between variations in the intensity of the zonal circulation of the atmosphere and the displacements of the semi-permanent centers of action. *J. Mar. Res.*, **2**, 38–55, URL https://cir.nii.ac.jp/crid/1571135650851329280.

Röthlisberger, M., and O. Martius, 2019: Quantifying the Local Effect of Northern Hemisphere Atmospheric Blocks on the Persistence of Summer Hot and Dry Spells. *Geophysical Research Letters*, **46 (16)**, 10 101–10 111, doi:10.1029/

2019GL083745, URL https://onlinelibrary.wiley.com/doi/abs/10.1029/2019GL083745, _eprint: https://onlinelibrary.wiley.com/doi/pdf/10.1029/2019GL083745.

Scherrer, S. C., M. Croci-Maspoli, C. Schwierz, and C. Appenzeller, 2006: Two-dimensional indices of atmospheric blocking and their statistical relationship with winter climate patterns in the Euro-Atlantic region. *International Journal of Climatology*, **26 (2)**, 233–249, doi:10.1002/joc.1250, URL https://onlinelibrary.wiley.com/doi/abs/10.1002/joc.1250, _eprint: https://onlinelibrary.wiley.com/doi/pdf/10.1002/joc.1250.

Shutts, G. J., 1983: The propagation of eddies in diffluent jetstreams: Eddy vorticity forcing of 'blocking' flow fields. *Quarterly Journal of the Royal Meteorological Society*, **109 (462)**, 737–761, doi:10.1002/qj.49710946204, URL https://onlinelibrary.wiley.com/doi/abs/10.1002/qj.49710946204, _eprint: https://onlinelibrary.wiley.com/doi/pdf/10.1002/qj.49710946204.

Tachibana, Y., T. Nakamura, H. Komiya, and M. Takahashi, 2010: Abrupt evolution of the summer Northern Hemisphere annular mode and its association with blocking. *Journal of Geophysical Research: Atmospheres*, **115 (D12)**, doi:10.1029/2009JD012894, URL https://onlinelibrary.wiley.com/doi/abs/10.1029/2009JD012894, _eprint: https://onlinelibrary.wiley.com/doi/pdf/10.1029/2009JD012894.

Teng, H., G. Branstator, H. Wang, G. A. Meehl, and W. M. Washington, 2013: Probability of US heat waves affected by a subseasonal planetary wave pattern. *Nature Geoscience*, **6 (12)**, 1056–1061, doi:10.1038/ngeo1988, URL https://www.nature.com/articles/ngeo1988, number: 12.

Thompson, D. W. J., and J. M. Wallace, 2000: Annular Modes in the Extratropical Circulation. Part I: Month-to-Month Variability. *Journal of Climate*, **13 (5)**, 1000–1016, doi:10.

1175/1520-0442(2000)013⟨1000:AMITEC⟩2.0.CO;2, URL https://journals.ametsoc.org/view/journals/clim/13/5/1520-0442_2000_013_1000_amitec_2.0.co_2.xml.

Tyrlis, E., and B. J. Hoskins, 2008: Aspects of a Northern Hemisphere Atmospheric Blocking Climatology. *Journal of the Atmospheric Sciences*, **65 (5)**, 1638–1652, doi:10.1175/2007JAS2337.1, URL https://journals.ametsoc.org/view/journals/atsc/65/5/2007jas2337.1.xml.

Wang, L., and Coauthors, 2026: Gaps and Ways Forward in Atmospheric Blocking and Extreme Weather Research (Accepted). *Nature Communications*.

Wirth, V., M. Riemer, E. K. Chang, and O. Martius, 2018: Rossby Wave Packets on the Midlatitude Waveguide—A Review. *Monthly Weather Review*, **146 (7)**, 1965–2001, doi:10.1175/MWR-D-16-0483.1, URL https://journals.ametsoc.org/view/journals/mwre/146/7/mwr-d-16-0483.1.xml.

Woollings, T., and Coauthors, 2018: Blocking and its Response to Climate Change. URL https://link.springer.com/article/10.1007/s40641-018-0108-z.

LIST OF TABLES

TABLE 1. Blocking regions in ERA5

Region	**Season**	**Longitude Range**	**Latitude Range**
Northern Pacific	JJA	150°E–150°W	50°–70°N
Northern Pacific	DJF	120°E–180°E	45°–65°N
Northern Atlantic	JJA	60°W–0°	55°–75°N
Northern Atlantic	DJF	30°W–30°E	40°–60°N
Southern Pacific	DJF	170°E–130°W	70°–50°S
Southern Pacific	JJA	120°W–60°W	70°–50°S

TABLE 2. Blocking regions in CESM1 simulations

Region	**Season**	**Longitude Range**	**Latitude Range**
Northern Pacific	JJA	150°E–150°W	55°–75°N
Northern Pacific	DJF	120°E–180°E	45°–65°N
Northern Atlantic	JJA	60°W–0°	55°–75°N
Northern Atlantic	DJF	30°W–30°E	40°–60°N
Southern Pacific	DJF	170°E–130°W	65°–45°S
Southern Pacific	JJA	130°W–70°W	70°–50°S

TABLE 3. Blocking statistics in ERA5 and CESM1 model simulations

		Recurrence (day)			**Duration (day)**		
Region	**Season**	ERA5	CTRL	RCP 8.5	ERA5	CTRL	RCP 8.5
Northern Pacific	JJA	8.4	9.3 ‘	10.4	8.2	8.3	8.1
Northern Atlantic	JJA	11.4	9.7	9.6	7.5	7.4	8.0
Southern Pacific	DJF	9.9	7.4	8.3	7.9	7.7	7.1
Northern Pacific	DJF	8.1	7.6	7.5	7.4	7.8	7.5
Northern Atlantic	DJF	8.9	7.8	8.1	8.2	8.1	7.8
Southern Pacific	JJA	11.9	8.9	8.8	7.1	7.5	7.4

TABLE 4. Statistics for return period distributions in ERA5 and red noise model

Region	**Season**	ϕ	**Onset freq, ERA5 (‰)**	**Onset freq, model (‰)**	**p-value (mean)**	**KL-div**
Northern Pacific	JJA	0.71	5.12	5.14	0.130	0.041
Northern Atlantic	JJA	0.66	4.37	4.44	0.221	0.050
Southern Pacific	DJF	0.66	4.30	4.35	0.005	0.029
Northern Pacific	DJF	0.63	5.39	5.37	0.050	0.075
Northern Atlantic	DJF	0.78	4.06	3.91	0.112	0.050
Southern Pacific	JJA	0.61	3.08	3.03	0.016	0.069

TABLE 5. Statistics for return period distributions in CESM1 simulations

Region	**Season**	ϕ, **CTRL**	ϕ, **RCP 8.5**	**Onset freq, CTRL (%)**	**Onset freq, RCP 8.5 (%)**	**p-value (mean)**	**KL-div**
Northern Pacific	JJA	0.79	0.82	4.09	3.10	0.01	0.019
Northern Atlantic	JJA	0.72	0.72	3.32	3.45	0.42	0.006
Southern Pacific	DJF	0.67	0.65	3.32	2.63	0.18	0.011
Northern Pacific	DJF	0.76	0.76	4.24	3.69	0.34	0.009
Northern Atlantic	DJF	0.83	0.81	3.04	2.78	0.22	0.012
Southern Pacific	JJA	0.73	0.68	3.51	3.53	0.30	0.004

LIST OF FIGURES

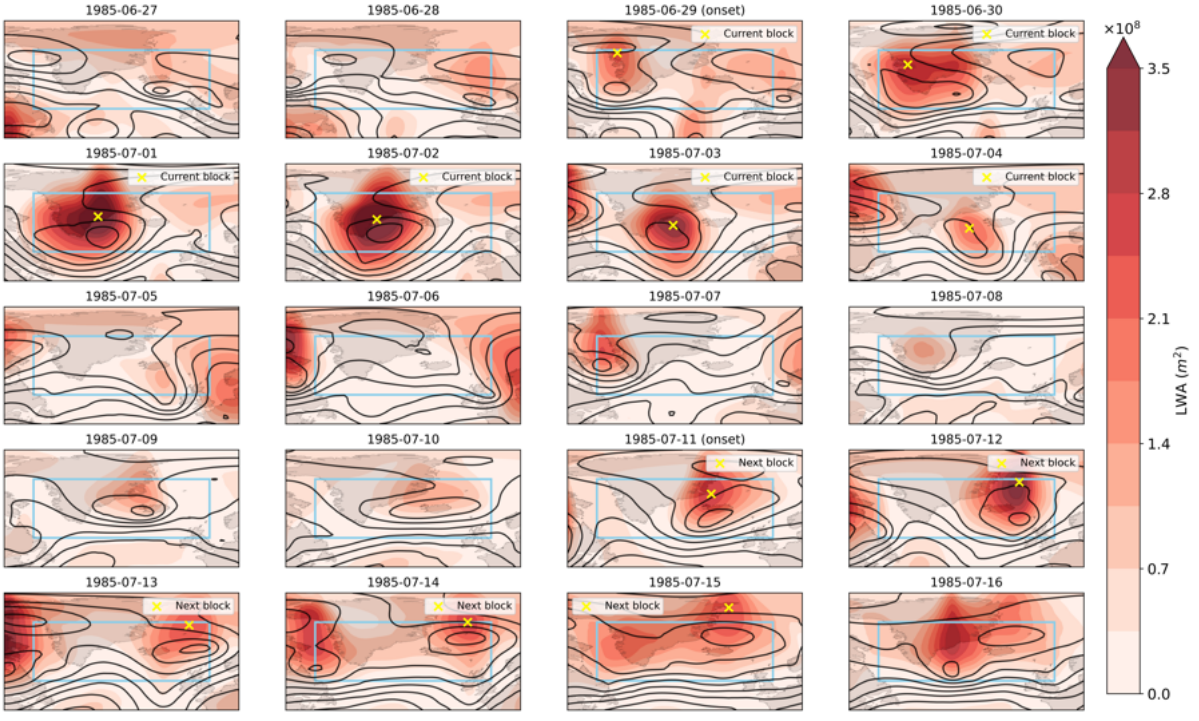

FIG. 1. Z500 contour plots with LWA shading showing a recurring blocking episode over the Northern Atlantic on 29 June 1985 and 11 July 1985. Event tracking points are marked by yellow crosses, and the region used for the return period calculation is indicated by the blue box. Z500 contours range from 5000 to 5975 m at 75 m intervals

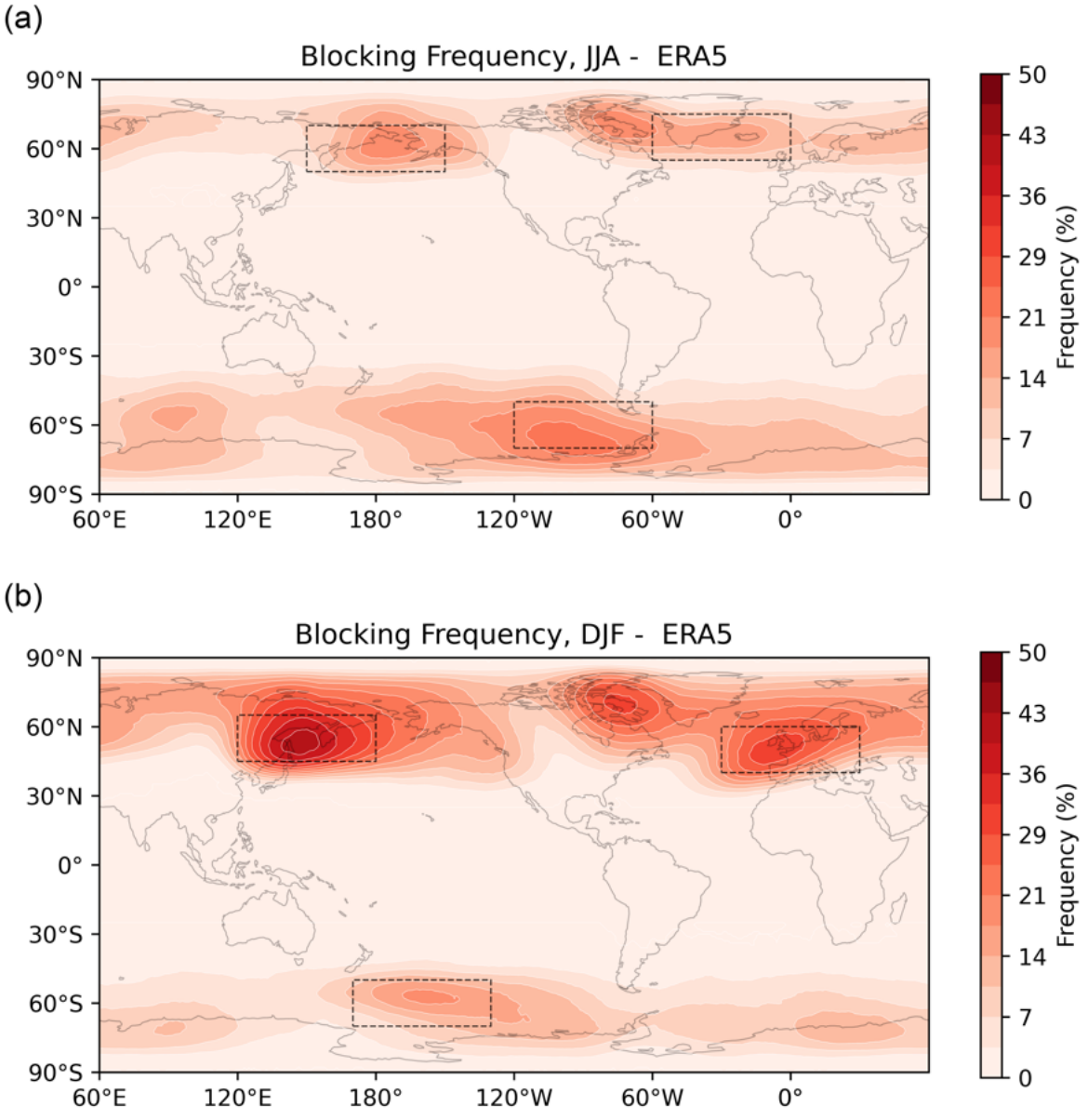

598 FIG. 2. The percentage of time the flow is blocked, as a function of latitude and longitude, in ERA5 reanalysis
599 over the period 1940–2022 for (a) JJA and (b) DJF. Regions used for recurrence analysis in ERA5 are indicated
600 by boxes.

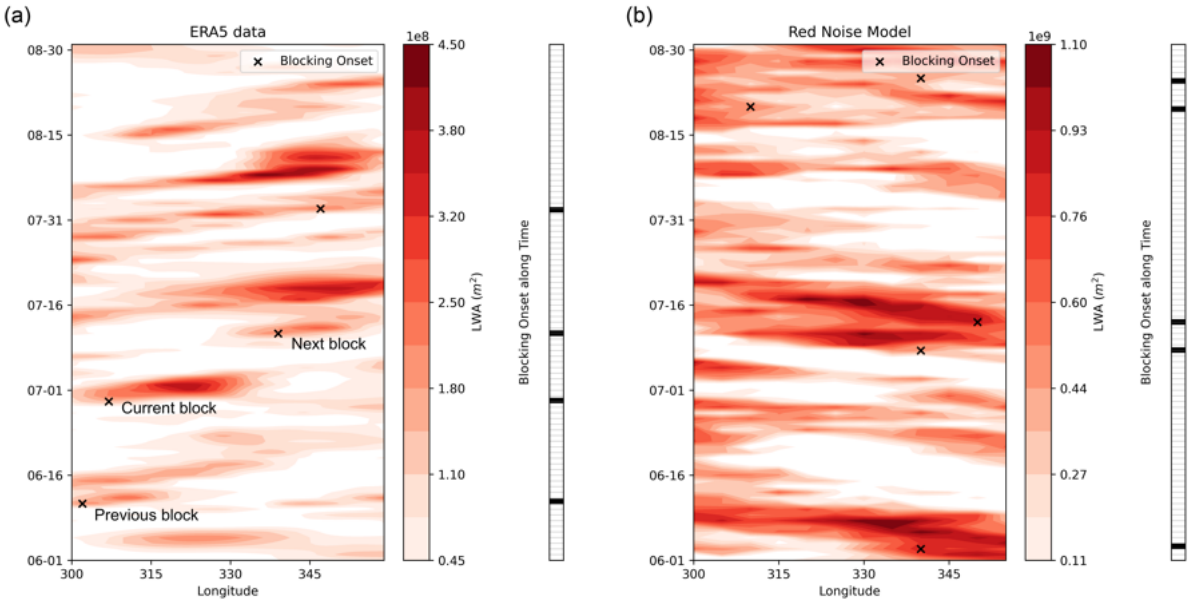

FIG. 3. Hovmöller diagram of LWA from (a) ERA5 in 1985 JJA and (b) the red noise model for the Northern Atlantic region (150ºE-150ºW). The LWA from ERA5 has been averaged over latitudes 55º-77ºN. Blocking onsets are marked by crosses, between which the return period is defined. They are also indicated on the 1D timeline array to the right of each diagram.

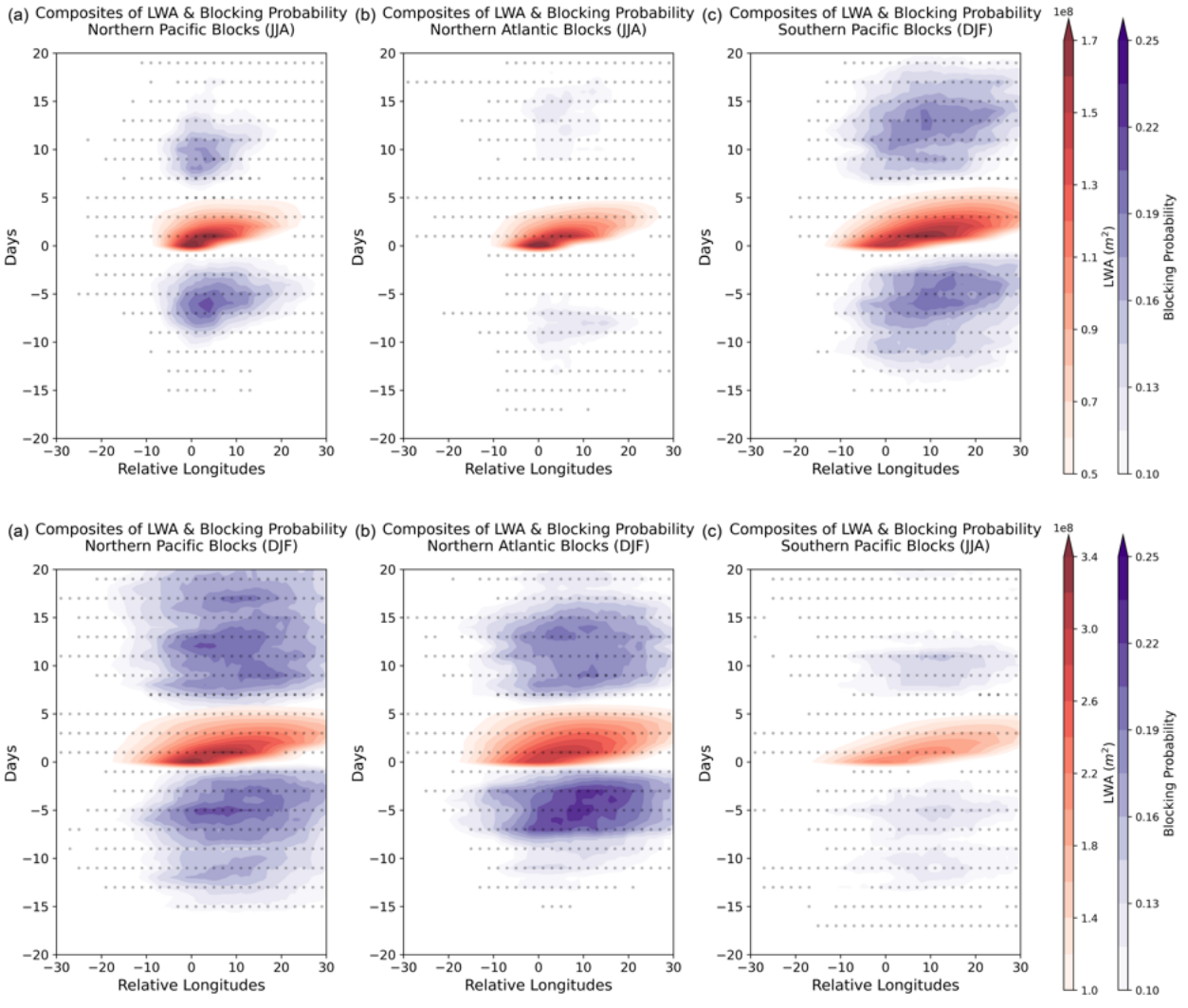

FIG. 4. Composites of LWA from ERA5 in the Northern Pacific (left), Northern Atlantic (middle), and Southern Pacific (right) for boreal/austral summer (a–c) and winter (d–f). Red shading shows LWA associated with blocking events, centered on the onset day and aligned by the longitude of the reference tracking point, with values averaged over ±5° latitude. Purple shading indicates the fraction of time there was a preceding and subsequent blocking events at the location and lead/lag time. Black dots denote grid points significant at the 0.99 level.

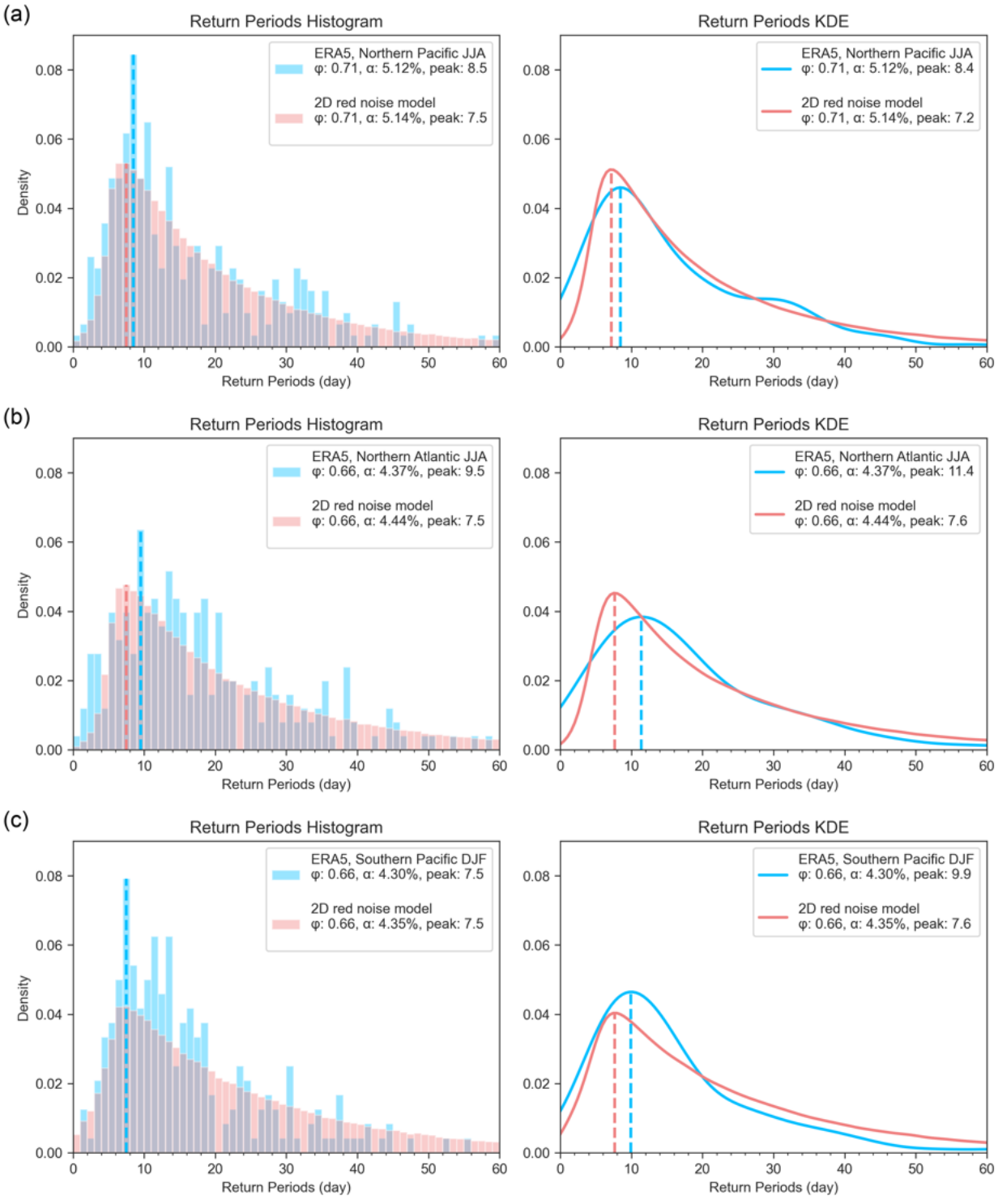

FIG. 5. Histograms and corresponding KDE plots of return periods from ERA5 (blue) and corresponding ERA5-constrained 2D red noise model (red) during summertime for (a) Northern Pacific, (b) Northern Atlantic and (c) Southern Pacific regions. Dashed lines mark the peaks of the histograms and KDE curves, indicating the recurrence timescale

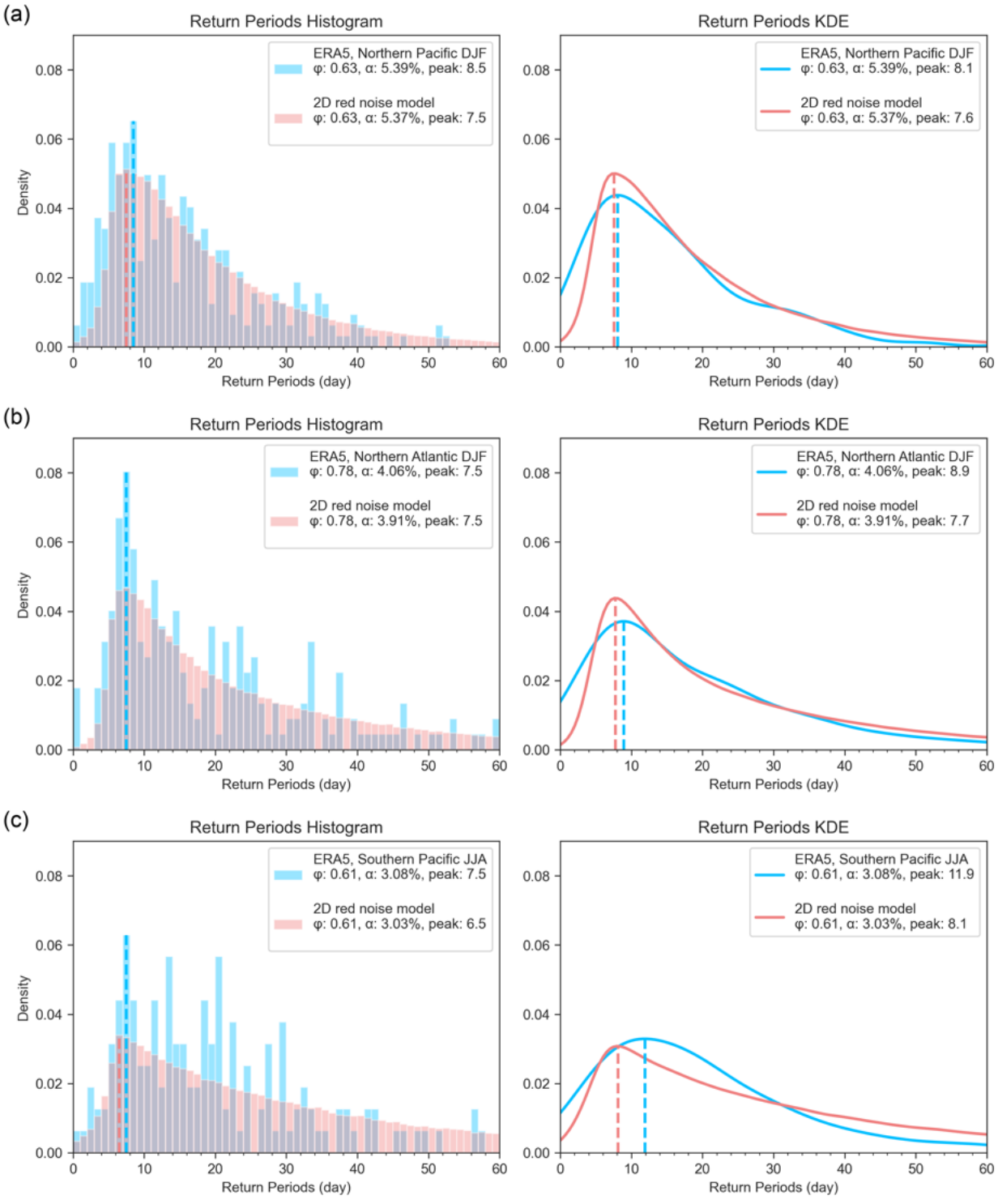

FIG. 6. Histograms and corresponding KDE plots of return periods from ERA5 (blue) and corresponding ERA5-constrained 2D red noise model (red) during wintertime for (a) Northern Pacific, (b) Northern Atlantic, and (c) Southern Pacific regions. Dashed lines mark the peaks of the histograms and KDE curves, indicating the recurrence timescale

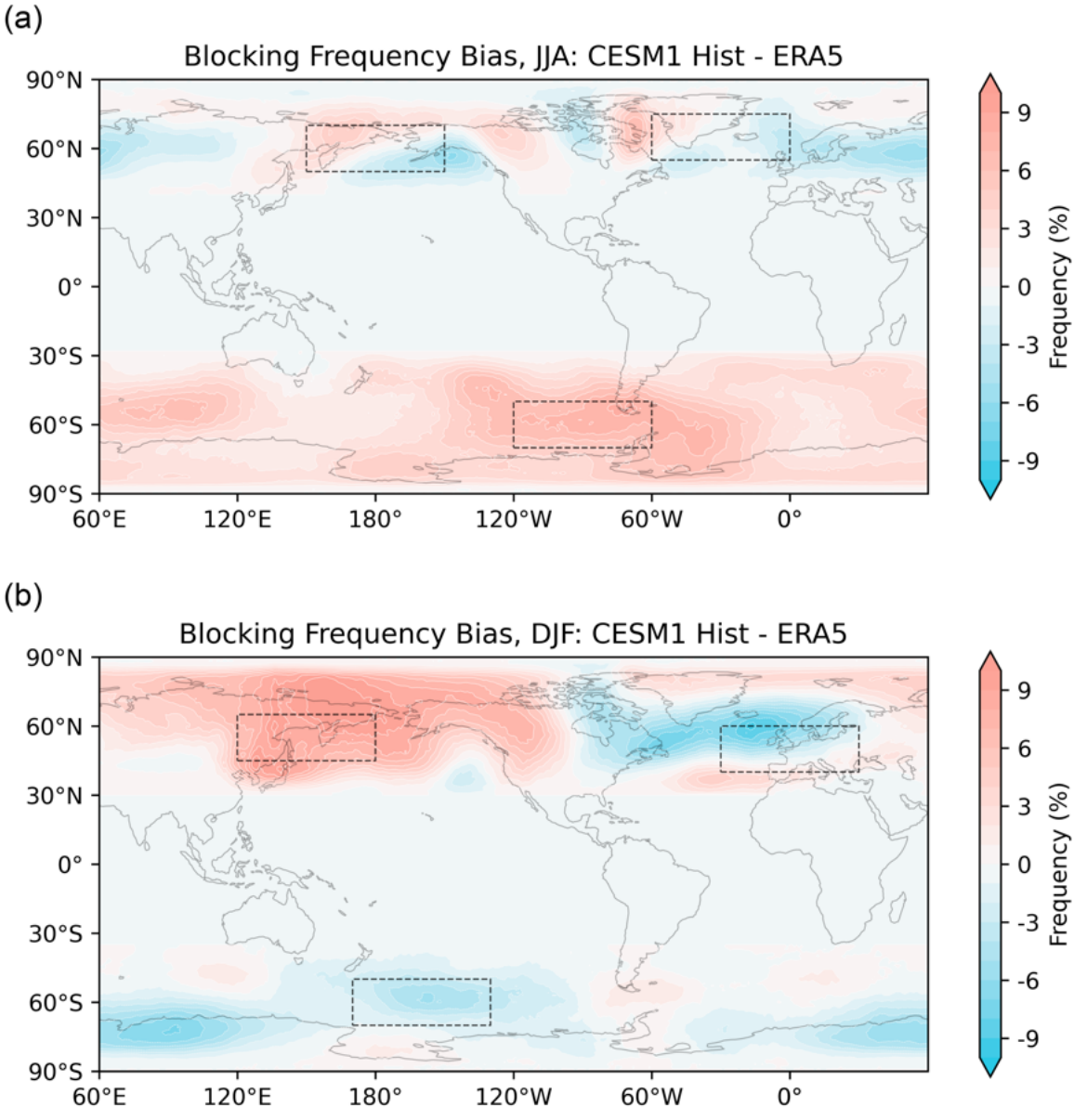

619 FIG. 7. Blocking frequency bias from CESM1 Hist CTRL simulation for (a) JJA and (b) DJF. Regions used
620 for recurrence analysis in ERA5 are indicated by boxes.

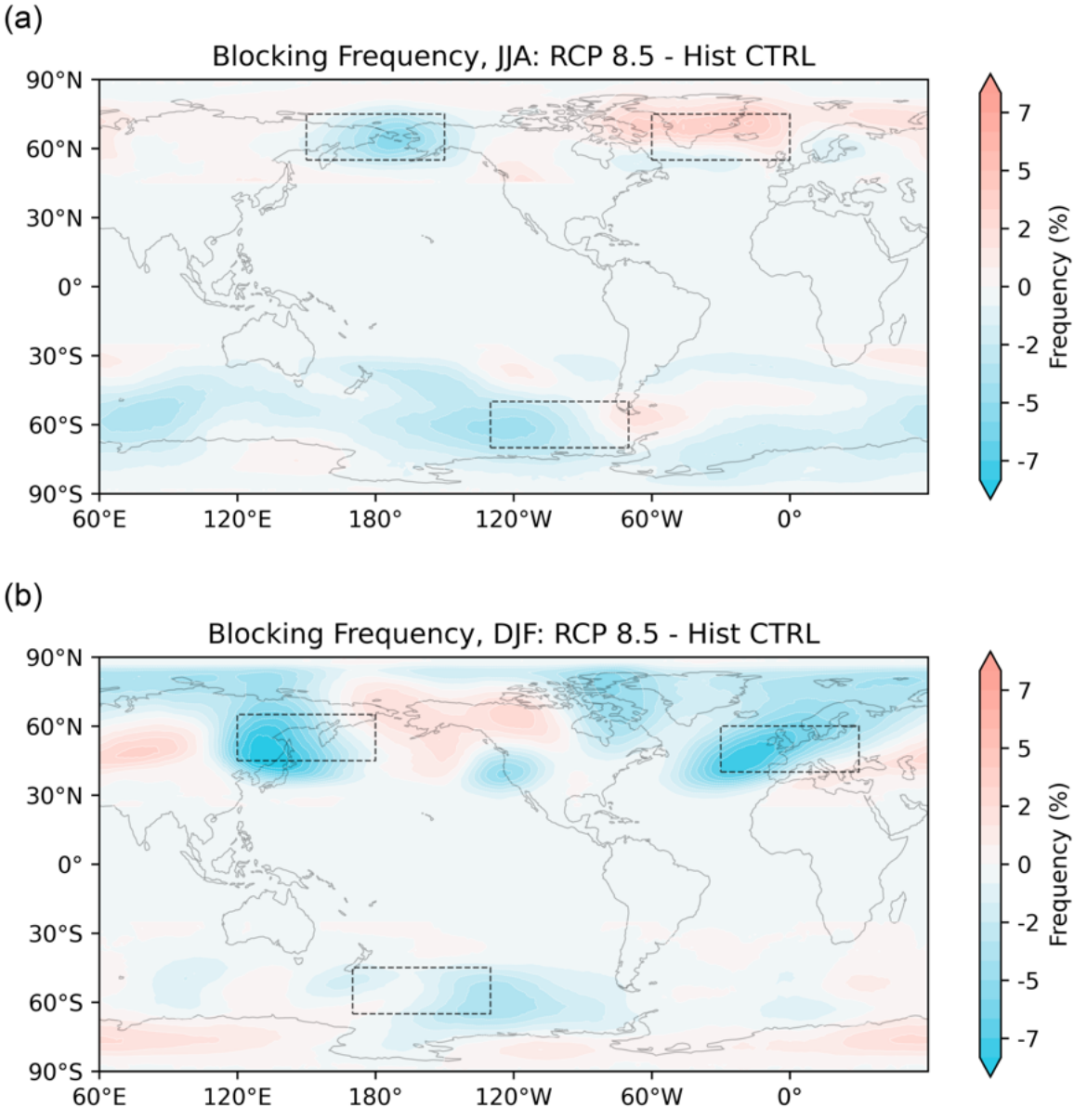

621 FIG. 8. Blocking frequency response from CESM1 simulations for (a) JJA and (b) DJF. Regions used for
622 recurrence analysis in CESM1 are indicated by boxes.

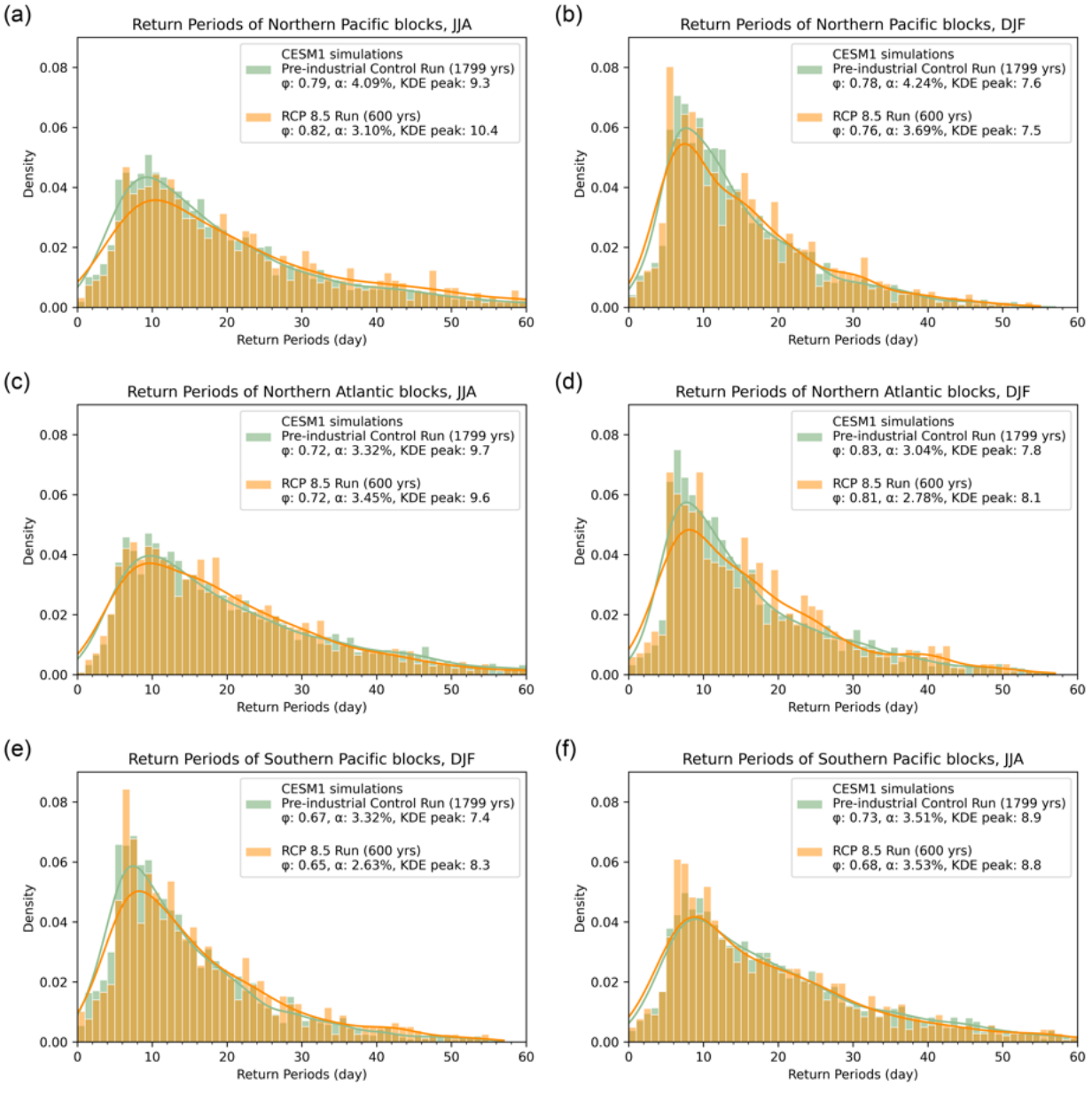

FIG. 9. Histograms and corresponding KDE curves of return periods from CESM1 model for preindustrial control simulation (green) and RCP 8.5 simulation (orange) during summer and wintertime for (a-b) Northern Pacific, (c-d) Northern Atlantic, and (e-f) Southern Pacific regions

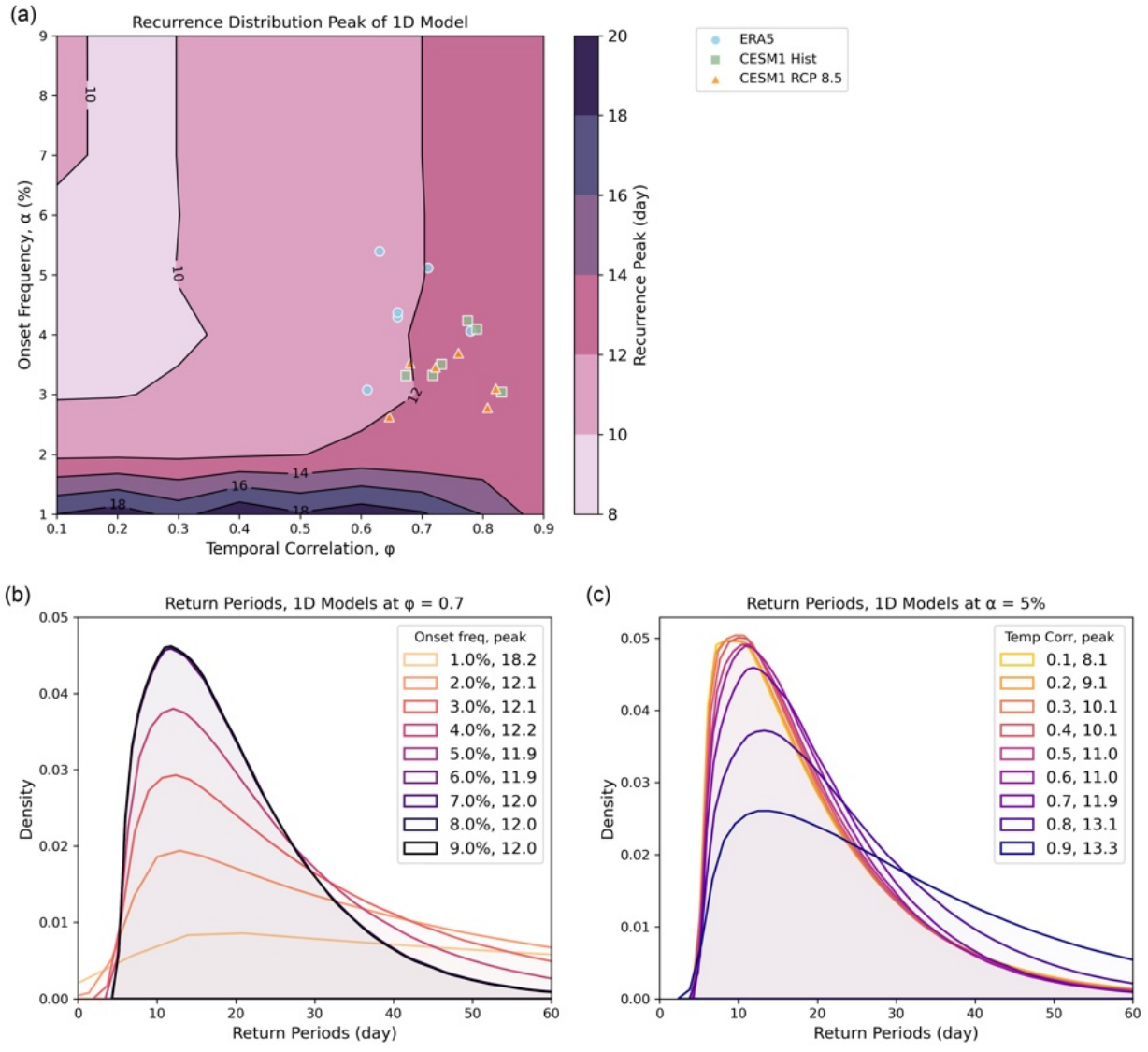

FIG. 10. (a) Table of recurrence peaks for the 1D conceptual red noise models across temporal correlations and onset frequency, with markers indicating temporal correlation coefficients and onset frequencies from ERA5 (blue circle), CESM pre-industrial run (green square) and RCP 8.5 run (orange triangle), (b) return period distributions across onset frequencies at temporal correlation, $\phi = 0.7$, and (c) return period distributions across temporal correlations at onset frequency, $\alpha = 5\%$ for the 1D red noise models

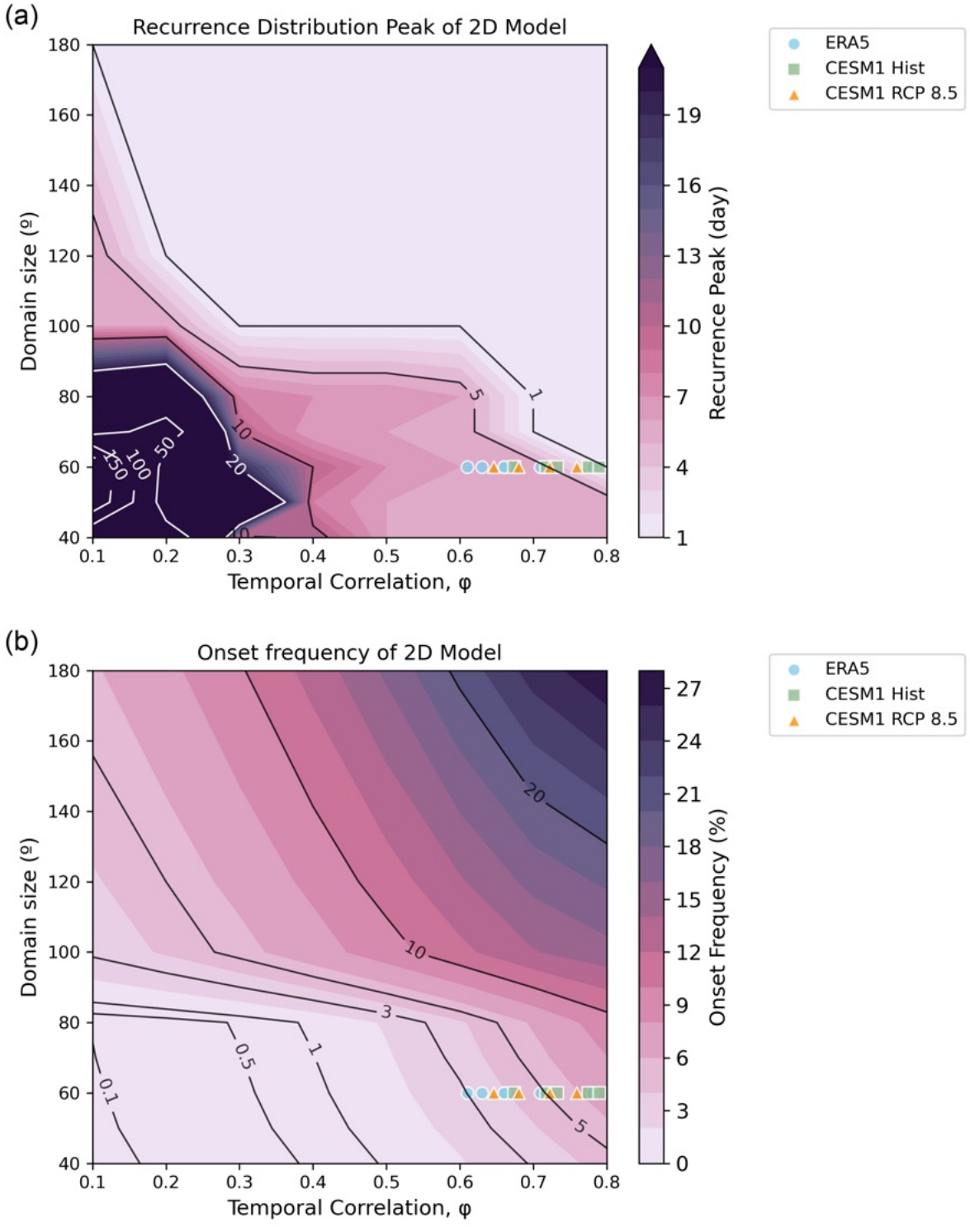

631 FIG. 11. (a) Table of recurrence peaks and (b) onset frequency for the 2D conceptual red noise models across
632 temporal correlations and domain sizes, with markers indicating temporal correlation coefficients and domain
633 size from ERA5 (blue circle), CESM pre-industrial run (green square) and RCP 8.5 run (orange triangle)

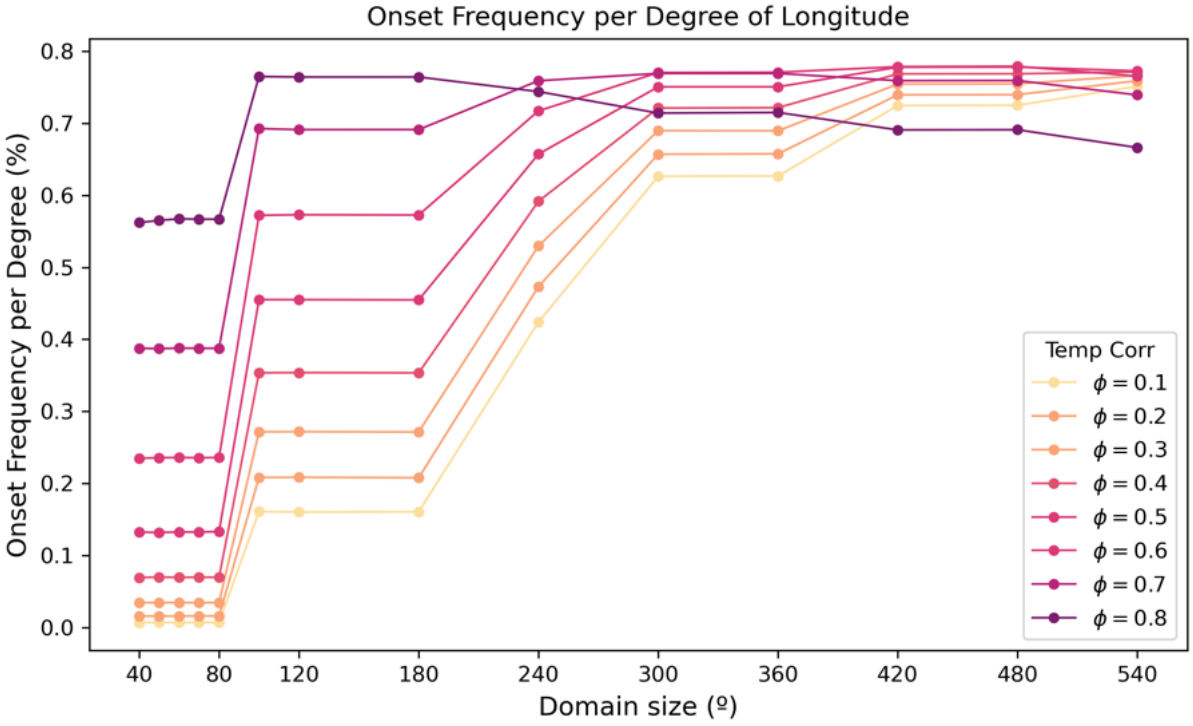

634 FIG. 12. Onset frequency per degree in longitude across domain sizes at different temporal correlations in the
635 2D red noise conceptual models

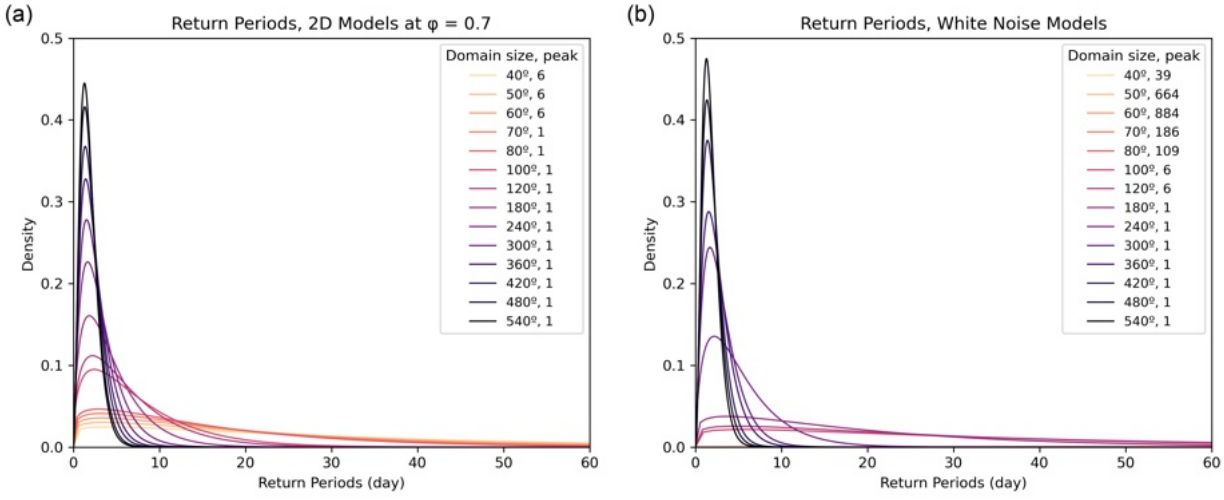

FIG. 13. (a) Return period distributions (with gamma fitting) in the 2D conceptual red noise models across domain sizes at temporal correlation, ϕ = 0.7, and (b) return period distributions (with gamma fitting) in 2D white noise models across domain sizes

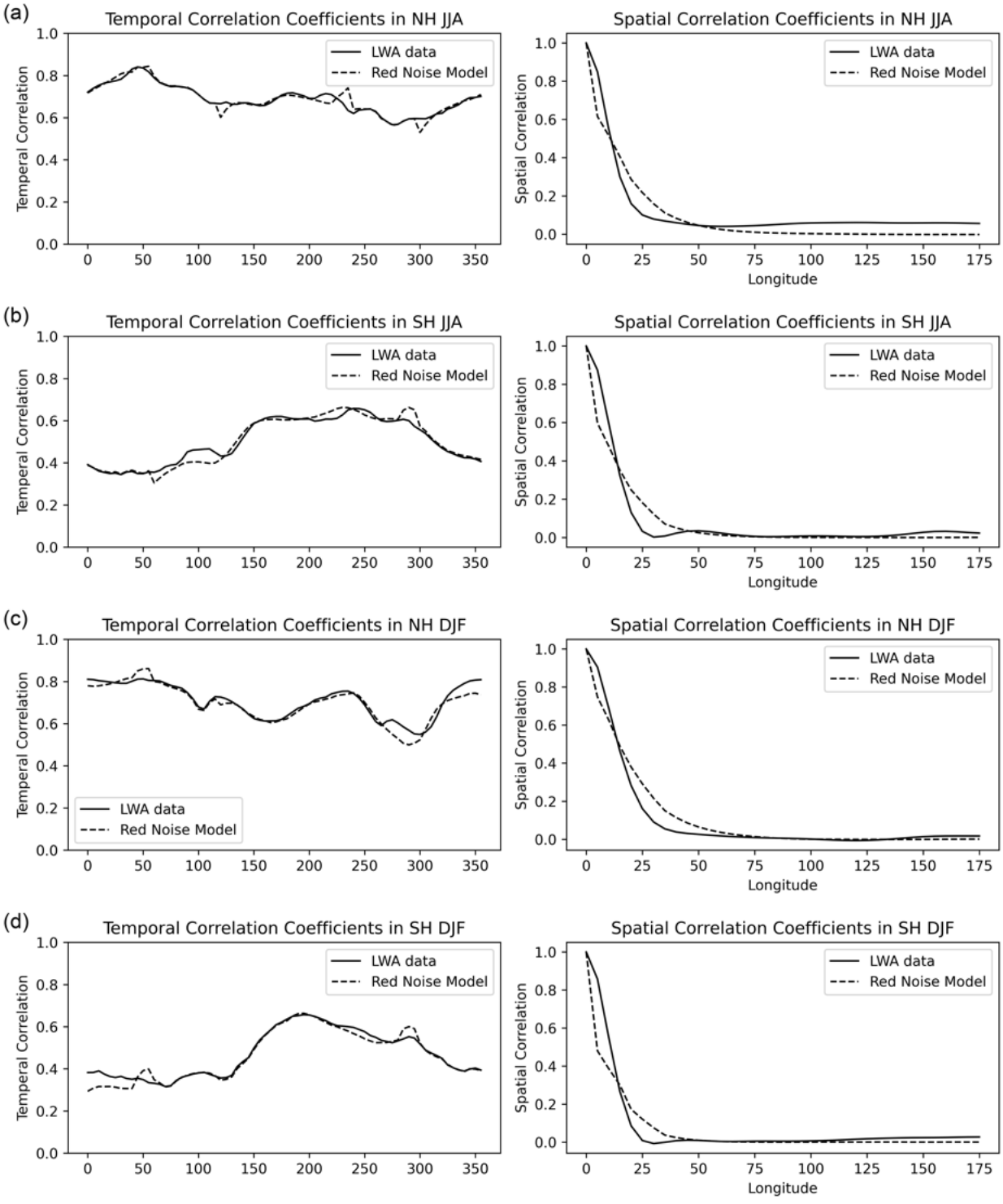

639 FIG. 14. Temporal and spatial correlations of LWA in ERA5 (solid) and the ERA5-constrained 2D red noise
640 model (dotted) in both hemispheres during (a-b) JJA and (c-d) DJF